Theoretical simulation study of linearly polarized light on microscopic second-harmonic generation in collagen type I

Ying Chang
Changshui Chen
South China Normal University
MOE Key Laboratory of Laser Life Science
Shipai
Guangzhou, Guangdong 510631
China

Jianxin Chen
Fujian Normal University
Institute of Laser and Optoelectronics Technology
Fujian Provincial Key Laboratory for Photonics Technology
Key Laboratory of Optoelectronic Science and Technology for Medicine of Ministry of Education
No. 8 Shangshan Road
Fuzhou, Fujian 350007
China

Ying Jin
Xiaoyuan Deng
South China Normal University
MOE Key Laboratory of Laser Life Science
Shipai
Guangzhou, 510631
China

Abstract. A theoretical model is established for dealing with second-harmonic generation (SHG) in type I collagen excited by linearly polarized light focused by a microscope. With this model, the effects of the polarization angle α, numerical aperture (NA), as well as the ratio of hyperpolarizability $\rho=\beta_{xxx}/\beta_{xyy}$ on SHG emission have been investigated. Simulation results reveal that SHG emission power changes periodically as α. The use of lower NA leads to weaker SHG emission but is more concentrated in two closer lobes, whereas more distributed emission in two detached lobes appear at higher NA. As the introduction of polarization direction, which is not along with the fiber axis ($\alpha \neq 0$ deg), one more element β_{xyy} is valid in our case than β_{xxx} alone, while their ratio ρ plays a very important role for collagen features characterization. SHG emission with ρ shows complicated modality that SHG emission is different at different α and not symmetric at $\pm\rho$ except at $\alpha=0$ deg, suggesting the important impact of polarization working on ρ for SHG emission. Our theoretical simulation results provide useful clues for experimental study of microscopic SHG emission in collagen excited by linearly polarized beam. [DOI: 10.1117/1.3174427]

Keywords: second-harmonic generation (SHG); polarization (α); numerical aperture (NA); hyperpolarizabilities (β).

Paper 09014R received Jan. 15, 2009; revised manuscript received May 11, 2009; accepted for publication May 28, 2009; published online Jul. 27, 2009.

1 Introduction

Second-harmonic generation (SHG) microscopy, based on radiative SHG under a focused beam has attracted more and more interest because it has been proved to be a powerful tool for visualization of cell and tissue structures and functions with microresolution.[1,2]

Collagen has the particular relevance of microscopic SHG applications onto biological imaging.[3,4] Collagen is the most abundant intrinsic structural protein in tissues. Collagen has a highly crystalline triple-helix structure, which is not centrosymmetric,[5,6] and the molecules are organized on the scale of the wavelength of light, which suggests that collagen is a promising biomedical material capable of SHG. Meanwhile, collagen possesses first hyperpolarizabilities β large enough for practical SHG.[7]

SHG in collagen fiber has been widely investigated, experimentally and theoretically. However, although many experiments on SHG in collagen have been accomplished under the microscope, theoretically, SHG in collagen under a focused beam has far from thorough investigation, such as the polarization effect. Thus far, polarization effect on SHG under focused beam has been investigated only on uniformly distributed dye dipoles on a planar cell membrane.[8] In collagen, such studies have been concentrated on the excitation by collimated light rather than focused light.[9,10] Under a focused beam, only in a very special condition, such as the excitation beam, which polarizes parallel to the fibril axis, has been dealt with.[11] SHG is a nonlinear optical phenomenon involving coherent photon scattering. Because of the coherent nature of SHG, the radiation of SHG is usually highly directional and depends critically on the emission source, such as its spatial extent, polarization of the excitation electric field.[12,13] Also, we realize that collagen fiber has its own physical properties compared to the uniformly distributed dipole on surface, and in practice, the polarization of the excitation light relative to the collagen fiber axis is indeterminable because of the unknown sample-laid position. It is therefore desirable for the theoretical exploration of SHG emission under the polarized focused beam on collagen fibrils.

Moreover, it is well known that the structure of collagen plays an important role in various pathological processes and diseases, such as wound healing, malignancy, or development,[14] and SHG microscopy can be accomplished *in vivo*. Thus, this theoretical analysis exhibits promise for biomedical assessment of tissue structure, especially in patho-

Address all correspondence to: Xiaoyuan Deng, MOE Key Laboratory of Laser Life Science, South China Normal University, Guangzhou, 510631, China. Tel: 86-158 1881 4678; Fax: 86-20-8521 0889; E-mail: xiaoyuandeng@gmail.com

1083-3668/2009/14(4)/044016/12/$25.00 © 2009 SPIE

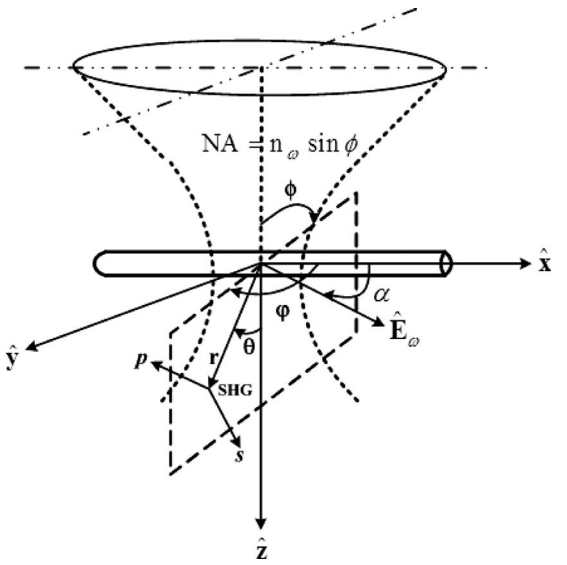

Fig. 1 Schematic diagram defining SHG emission from collagen under linearly polarized focused beam. Collagen fiber is assumed along the $\vec{x}$ direction. The fibrils within the fiber are generally aligned to the fiber axis. The light is linearly polarized in x-y plane ($\vec{E}_\omega$) with the angle of α from $\vec{x}$ direction and propagates in the $\vec{z}$ direction. SHG propagates in the emission plane, defined by (θ, φ).

logical processes where the collagen is being actively remodeled.

Therefore, in this paper, we aim to explore the effects of polarized focused excitation beam on SHG in collagen. A single fibril is applied as the collagen model in this paper.

2 Theory of SHG Field Propagation under a Linearly Polarized Focused Beam

We consider here an illumination beam focusing on to the collagen fiber through a microscopic objective with the numerical aperture of NA$=n_\omega \sin\phi$. The light is linearly polarized in the x-y plane ($\vec{E}_\omega$) with the angle of α from the $\vec{x}$ direction and propagates in the $\vec{z}$ direction with an angular frequency of ω. Collagen fiber is assumed along the $\vec{x}$ direction. The fibrils within the fiber are generally aligned to the fiber axis, and the nonlinear scatterers (dipoles) are distributed uniformly within the collagen fibrils. The diagram of coordinate system for calculating the SHG field at an observation point (r, θ, φ) is shown in Fig. 1.

2.1 *Electric-field $\vec{E}_\omega$ Profile of the Linearly Polarized Focused Beam*

The local field distribution of excitation beam within the focus is very important for the determination of the propagation direction of the SHG field. For nonlinear applications, a linearly polarized, $\vec{z}$-directed beam at the focus can be well approximated by a three-dimensional Gaussian profile as follows:[15]

$$\vec{E}_\omega(x,y,z) = -i\vec{E}_\omega^{(0)} \exp\left(-\frac{x^2+y^2}{w_{xy}^2} - \frac{z^2}{w_z^2} + i\xi k_\omega z\right)\hat{\varepsilon}, \quad (1a)$$

$$\vec{E}_\omega^{(0)} = \vec{E}_\omega(0,0,0), \quad (1b)$$

where $\vec{E}_\omega(x,y,z)$ is the complex amplitude of the driving field at the point (x,y,z), $\hat{\varepsilon}$ represents its polarization direction ($\varepsilon_z=0$ in our case). $k_\omega=2\pi n_\omega/\lambda_\omega$ is the wave vector in a specimen with a refractive index of n_ω. ξ is the wave-vector reduction factor due to focusing that accounts for a reduction in axial momentum by conversion to lateral momentum components within the focus. w_{xy} and w_z are the $1/e$ radii of the focal ellipse in the lateral and axial directions, respectively.[1]

$$w_{xy} = \begin{cases} \dfrac{0.320\lambda_\omega}{\mathrm{NA}} & \mathrm{NA} \leqslant 0.7 \\ \dfrac{0.325\lambda_\omega}{\mathrm{NA}^{0.91}} & \mathrm{NA} > 0.7 \end{cases}, \quad (2a)$$

$$w_z = 0.532\lambda_\omega \left[\frac{1}{n_\omega - \sqrt{n_\omega^2 - \mathrm{NA}^2}}\right]. \quad (2b)$$

2.2 *Induced Dipole Moment of SHG*

The total dipole moment $\vec{\mu}$ induced by the field $\vec{E}_\omega$ is often written as a Taylor series[16]

$$\vec{\mu} = \vec{\mu}_0 + \alpha\cdot\vec{E}_\omega + \frac{1}{2!}\beta\cdot\vec{E}_\omega^2 + \frac{1}{3!}\gamma\cdot\vec{E}_\omega^3 + \cdots. \quad (3)$$

Here, $\vec{\mu}_0$ is the permanent dipole moment, the frequency dependent α, β, and γ are the linear polarizability, and the first and second hyperpolarizability, respectively. SHG is related to the third term, and the total local dipole moment per unit scatterer concentration can be expressed in more detail as[8]

$$\vec{\mu}_{2\omega,i}(x,y,z) = \frac{1}{2}\vec{E}_\omega^2(x,y,z)\sum_{j,k}\langle\beta_{ijk}\rangle\hat{\varepsilon}_j\hat{\varepsilon}_k, \quad (4)$$

where $\langle\beta\rangle$ symbolizes a local ensemble average of the fibril hyperpolarizabilities. Under the assumption of Kleinman and cylindrical symmetry (please see the Appendix A), dipole moment introduced by electric field $\vec{E}_\omega$ along the $\vec{x}$ and $\vec{y}$ direction is respectively to be

$$\mu_{2\omega,x}(x,y,z) = \tfrac{1}{2}E_\omega^2(x,y,z)(\beta_{xxx}\varepsilon_x\varepsilon_x + \beta_{xyy}\varepsilon_y\varepsilon_y), \quad (5a)$$

$$\mu_{2\omega,y}(x,y,z) = \tfrac{1}{2}E_\omega^2(x,y,z)(\beta_{xyy}\varepsilon_x\varepsilon_y + \beta_{xyy}\varepsilon_x\varepsilon_y). \quad (5b)$$

In particular, for a linearly polarized beam at an angle α with respect to the collagen fiber produces the SHG dipole moment as follows:

$$\vec{\mu}_{2\omega}(x,y,z)=\begin{pmatrix}\mu_{2\omega,x}(x,y,z)\\ \mu_{2\omega,y}(x,y,z)\\ \mu_{2\omega,z}(x,y,z)\end{pmatrix}=\frac{1}{2}\vec{E}_{\omega}^{2}(x,y,z)\times\begin{pmatrix}\beta_{xxx}\varepsilon_x\varepsilon_x+\beta_{xyy}\varepsilon_y\varepsilon_y\\ \beta_{xyy}\varepsilon_x\varepsilon_y+\beta_{xyy}\varepsilon_y\varepsilon_x\\ 0\end{pmatrix}=\frac{1}{2}\vec{E}_{\omega}^{2}(x,y,z)\times\begin{pmatrix}\beta_{xxx}\cos^2\alpha+\beta_{xyy}\sin^2\alpha\\ \beta_{xyy}\sin 2\alpha\\ 0\end{pmatrix}=\frac{1}{2}\vec{E}_{\omega}^{2}(x,y,z)\beta. \tag{6}$$

2.3 *Induced Electric Field $\vec{E}_{2\omega}$ of SHG*

Following the achievement of the induced SHG dipole moment, we proceed to calculate the second-harmonic far field radiated in the direction (θ,φ) based on the coordinate system illustrated in Fig. 1. Far from the dipole, where it is called the wave or radiation zone, the configuration of $\vec{E}_{2\omega}$ is as follows:[17]

$$\vec{E}_{2\omega}(\psi)=\frac{\vec{\mu}_{2\omega}\omega^2}{\pi\varepsilon_0 c^2 r}\sin(\psi)\exp(-i\vec{k}_{2\omega}\cdot\vec{r})\hat{\psi}, \tag{7}$$

where ψ represents the angle between the $\vec{x}$-axis and the emission direction $\vec{r}$ of SHG. $\sin\psi=(\sin^2\theta\sin^2\varphi+\cos^2\theta)^{1/2}$ illustrates the projection relationship between the direction of emission SHG dipole moment $\vec{\mu}_{2\omega}$ and the excitation electric field $\vec{E}_{2\omega}$ of SHG. We define $\eta=\omega^2/\pi\varepsilon_0 c^2$, where ε_0 is the spree-space permittivity, c is the speed of light, and ω is the frequency of fundamental beam.

The total radiated second-harmonic signal in the far field is the integrated one from all scatterers that have the dipole volume density defined by N_V. Presented in polar coordinates, $\vec{E}_{2\omega}$ is described as follows:

$$\vec{E}_{2\omega}(\theta,\varphi)=\frac{\eta N_V}{r}\int\int\int \sin\psi\cdot\vec{\mu}_{2\omega}(x,y,z)\exp[-ik_{2\omega}(z\cos\theta+y\sin\theta\sin\varphi+x\sin\theta\cos\varphi)]dxdydz=\frac{\eta N_V}{r}(\sin^2\theta\sin^2\varphi+\cos^2\theta)^{1/2}\int\int\int\frac{1}{2}\beta\vec{E}_{\omega}^{(0)2}\exp\left(-2\frac{x^2+y^2}{w_{xy}^2}-2\frac{z^2}{w_z}+2i\xi k_{\omega}z\right)\times\exp[-ik_{2\omega}(z\cos\theta+y\sin\theta\sin\varphi+x\sin\theta\cos\varphi)]dxdydz. \tag{8}$$

(Derivation from Eq. (8) and (9), see Appendix B).

$$\vec{E}_{2\omega}(\theta,\varphi)=\left(\sqrt{\frac{\pi}{2}}\right)^3 N_V w_{xy}^2 w_z\frac{\eta}{r}(\sin^2\theta\sin^2\varphi+\cos^2\theta)^{1/2}\cdot\vec{\mu}_{2\omega}^{(0)}\times\exp\left\{-\frac{k_{2\omega}^2}{8}[w_{xy}^2(\sin\theta\cos\varphi)^2+w_{xy}^2(\sin\theta\sin\varphi)^2+w_z^2(\cos\theta-\xi')^2]\right\}=N\vec{E}_{2\omega}^{(0)}A(\theta,\varphi), \tag{9}$$

where the introduced parameters are

$$\vec{\mu}_{2\omega}^{(0)}=\begin{pmatrix}\mu_{2\omega,x}^{(0)}\\ \mu_{2\omega,y}^{(0)}\\ \mu_{2\omega,z}^{(0)}\end{pmatrix}=\frac{1}{2}\vec{E}_{\omega}^{2}(0,0,0)\beta=\frac{1}{2}\vec{E}_{\omega}^{(0)2}\beta,$$

which represents the contribution from the local induced polarization per unit volume density to the radiated electric field at the flocal center only [indicated by the superscript (0)].

$$N=\left(\sqrt{\frac{\pi}{2}}\right)^3 w_{xy}^2 w_z N_V \tag{10}$$

$$\vec{E}_{2\omega}^{(0)}=\frac{\eta}{r}(\sin^2\theta\sin^2\varphi+\cos^2\theta)^{1/2}\cdot\vec{\mu}_{2\omega}^{(0)} \tag{11}$$

$$A=\exp\left\{-\frac{k_{2\omega}^2}{8}[w_{xy}^2(\sin\theta\cos\varphi)^2+w_{xy}^2(\sin\theta\sin\varphi)^2+w_z^2(\cos\theta-\xi')^2]\right\}=\exp\left\{-\frac{k_{2\omega}^2}{8}[w_{xy}^2\sin^2\theta+w_z^2(\cos\theta-\xi')^2]\right\}. \tag{12}$$

A is the angular modulation term.

$N=VN_V$, and $V=(\sqrt{\pi/2})^3 w_{xy}^2 w_z$ is the active SHG volume.[18] N defines as the effective total number of dipoles that contribute to the generation of second-harmonic light.

2.4 *Emission Direction of Electric Field of SHG*

Emission direction is confined by the emission plane (θ,φ). Electric field of SHG is normal to the observed direction $\vec{r}$. The radiated SHG with polarization components parallel (p) to and perpendicular (s) to this plane can be derived as follows:

$$\vec{E}_{2\omega}^{(0)}(\theta,\varphi)=\begin{pmatrix}E_{2\omega}^{(0)p}(\theta,\varphi)\\ E_{2\omega}^{(0)s}(\theta,\varphi)\end{pmatrix}=\frac{\eta}{r}\vec{M}\cdot\vec{\mu}_{2\omega}^{(0)}. \tag{13}$$

$\vec{M}$ is the projection matrix, which permutes coordinate (x,y,z) to (θ,φ). It is defined by

$$\vec{M}\begin{pmatrix}\vec{\theta}\\ \vec{\varphi}\end{pmatrix}=\begin{pmatrix}\cos\theta\cos\varphi & \cos\theta\sin\varphi & -\sin\theta\\ -\sin\varphi & \cos\varphi & 0\end{pmatrix}. \quad (14)$$

On the basis of Eq. (9), $E^p_{2\omega}(\theta,\varphi)$ and $E^s_{2\omega}(\theta,\varphi)$ is then derived from $\vec{E}^{(0)}_{2\omega}(\theta,\varphi)$. $E^p_{2\omega}$ is the amplitude of $\vec{E}_{2\omega}$ in the $\vec{\theta}$ direction and $E^s_{2\omega}$ is the amplitude of $\vec{E}_{2\omega}$ in the $\vec{\varphi}$ direction.[8]

However, in practice, the measurements of components of p and s directions of SHG are difficult because they are not fixed as the emission plane changes. On the contrary, SHG are more easily to be detected along the parallel ($\parallel$) and perpendicular ($\perp$) direction to the excitation polarization (α). Therefore, we further transform the (p,s) components to be $(\parallel,\perp)$ components through the following relationship:

$$\begin{pmatrix}E^{\parallel}_{2\omega}\\ E^{\perp}_{2\omega}\end{pmatrix}=\begin{bmatrix}\cos(\varphi-\alpha) & -\sin(\varphi-\alpha)\\ \sin(\varphi-\alpha) & \cos(\varphi-\alpha)\end{bmatrix}\begin{pmatrix}E^p_{2\omega}\\ E^s_{2\omega}\end{pmatrix}. \quad (15)$$

2.5 *Emission Power of SHG*

On the basis of the above derivation, the relationship of total power distribution of SHG with the electric-field strength presented in Eq. (9) can be further described to be (see Appendix C)

$$P_{2\omega}(\theta,\varphi)=\frac{1}{8}n_{2\omega}\varepsilon_0 c\,\eta^2A^2N^2E^{(0)4}_{\omega},$$

$$(1-\sin^2\theta\cos^2\varphi)\begin{pmatrix}\beta_{xxx}\cos^2\alpha+\beta_{xyy}\sin^2\alpha\\ \beta_{xyy}\sin 2\alpha\\ 0\end{pmatrix}^2. \quad (16)$$

By integrating Eq. (16) in solid angle, total power of SHG is derived, which only depends on the polarized direction α

$$\begin{aligned}P_{2\omega}&=\frac{1}{2}n_{2\omega}\varepsilon_0 c\,\eta^2N^2\Theta(\mu^{(0)2}_{2\omega,x}+\mu^{(0)2}_{2\omega,y}+\mu^{(0)2}_{2\omega,z})\\&=\frac{1}{8}n_{2\omega}\varepsilon_0 c\,\eta^2N^2\Theta E^{(0)4}_{\omega}[(\beta_{xxx}\cos^2\alpha+\beta_{xyy}\sin^2\alpha)^2\\&\quad+(\beta_{xyy}\sin 2\alpha)^2], \quad (17)\end{aligned}$$

where

$$\Theta=\int\int A^2(\theta,\varphi)(1-\sin^2\theta\cos^2\varphi)\sin\theta d\theta d\varphi,$$

Accordingly, the power distribution in parallel ($\parallel$) and perpendicular ($\perp$) components are as follows (see Appendix D):

$$\begin{aligned}P^{\parallel}_{2\omega}(\theta,\varphi)&=\frac{1}{2}n_{2\omega}\varepsilon_0 c r^2|E^{\parallel}_{2\omega}(\theta,\varphi)|^2\\&=\frac{1}{8}n_{2\omega}\varepsilon_0 c\,\eta^2N^2A^2(\theta,\varphi)E^{(0)4}_{\omega}\{\cos(\varphi-\alpha)\\&\quad\times[\cos\theta\cos\varphi(\beta_{xxx}\cos^2\alpha+\beta_{xyy}\sin^2\alpha)\\&\quad+\beta_{xyy}\cos\theta\sin\varphi\sin 2\alpha]-\sin(\varphi-\alpha)\\&\quad\times[-\sin\varphi(\beta_{xxx}\cos^2\alpha+\beta_{xyy}\sin^2\alpha)\\&\quad+\beta_{xyy}\cos\varphi\sin 2\alpha]\}^2, \quad (18a)\end{aligned}$$

$$\begin{aligned}P^{\perp}_{2\omega}(\theta,\varphi)&=\frac{1}{2}n_{2\omega}\varepsilon_0 c r^2|E^{\perp}_{2\omega}(\theta,\varphi)|^2\\&=\frac{1}{8}n_{2\omega}\varepsilon_0 c\,\eta^2N^2A^2(\theta,\varphi)E^{(0)4}_{\omega}\{\sin(\varphi-\alpha)\\&\quad\times[\cos\theta\cos\varphi(\beta_{xxx}\cos^2\alpha+\beta_{xyy}\sin^2\alpha)\\&\quad+\beta_{xyy}\cos\theta\sin\varphi\sin 2\alpha]+\cos(\varphi-\alpha)\\&\quad\times[-\sin\varphi(\beta_{xxx}\cos^2\alpha+\beta_{xyy}\sin^2\alpha)\\&\quad+\beta_{xyy}\cos\varphi\sin 2\alpha]\}^2. \quad (18b)\end{aligned}$$

SHG power in these two directions $(\parallel,\perp)$, respectively, can be calculated by integrating in solid angle as follows:

$$P^{\parallel}_{2\omega}=\int\int P^{\parallel}_{2\omega}(\theta,\varphi)\sin\theta d\theta d\varphi, \quad (19a)$$

$$P^{\perp}_{2\omega}=\int\int P^{\perp}_{2\omega}(\theta,\varphi)\sin\theta d\theta d\varphi. \quad (19b)$$

3 Simulation Study of Parameters of Linearly Polarized Focused Beam on SHG Emission

3.1 *Effects of Illumination Polarization on SHG Emission Power under Focused Beam*

In this section, we aim to explore the effects of illumination polarization on SHG emission power under focused beam. From the theoretical expression of total, parallel, and perpendicular SHG power in Eqs. (17), (19a), and (19b), we note that there remain two valid hyperpolarizability elements β_{xxx} and β_{xyy}. β_{xyy} is added in this situation due to the introduce of the illumination polarization α, which is not consistent with the fiber axis (α=0 deg). $\rho=\beta_{xxx}/\beta_{xyy}$ has been evaluated to vary between −3 to 3,[19] in this section, we take ρ to be 2.6 (type I collagen in rat liver) and further assume $\beta_{xyy}=1$ to simplify the model. The effect of $\rho=\beta_{xxx}/\beta_{xyy}$ is to be investigated in more detail in Sec. 3.3.

Fig. 2 shows the total $P_{2\omega}$, parallel $P^{\parallel}_{2\omega}$, and perpendicular $P^{\perp}_{2\omega}$ SHG emission power from collagen fiber as the change of polarization angle α with respect to fiber axis. All data are normalized by $(1/8)n_{2\omega}\varepsilon_0 c\,\eta^2N^2E^{(0)4}_{\omega}=1$. We can see from Fig. 2 that $P_{2\omega}$, $P^{\parallel}_{2\omega}$, and $P^{\perp}_{2\omega}$ SHG emission power change as the polarization angle α periodically. When polarization direction locates at α=0, 180, 360 deg, indicating that the polarization of the excited beam has the same direction as the

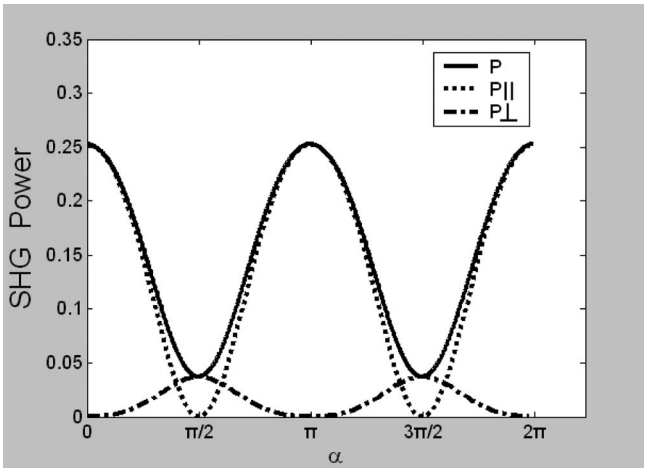

Fig. 2 Effects of polarization angle α on total $P_{2\omega}$, parallel $P_{2\omega}^{\parallel}$ and perpendicular $P_{2\omega}^{\perp}$ components of SHG emission power.

fibrils axis, the total power $P_{2\omega}$, and parallel $P_{2\omega}^{\parallel}$ power component achieve their maximum value, while the perpendicular $P_{2\omega}^{\perp}$ power component has its lowest value. On the contrary, we find that when the polarization of excited beam is perpendicular on the fibril axis (α=90, 270 deg) the total power $P_{2\omega}$ and parallel $P_{2\omega}^{\parallel}$ power component have their lowest value and perpendicular $P_{2\omega}^{\perp}$ component is the reverse. $P_{2\omega}$ and $P_{2\omega}^{\parallel}$ power component keep the similar configuration in amplitude and $P_{2\omega}^{\parallel}$ stands predominance in contribution to the SHG total power.

Parallel $P_{2\omega}^{\parallel}$ and perpendicular $P_{2\omega}^{\perp}$ power distribution along (θ,φ), using Eqs. (18a) and (18b), at polarization angles α=0, α=30, α=60, and α=90 deg, respectively have been demonstrated in three-dimension in Fig. 3. Basically, the parallel and perpendicular distribution of SHG emission possess two types of patterns. Under α=0, α=30, and α=60 deg conditions, these three parallel distribution has similar patterns, and the perpendicular one has another similar patterns; however, under the α=90 deg situation, the distribution shows reverse patterns in parallel and perpendicular components. As the polarization angle increases from α=0 to α=90 deg, SHG parallel emission power in the $\vec{z}$-axis (θ=0 deg) decreases, while the perpendicular one increases. Although the emission distribution pattern of the parallel component at α=90 deg and that of perpendicular components at α=0 deg are very similar, their amplitude is still slight different, which indicates that although the relative direction of measurement direction and fibril axis is the same as the above two conditions (which is perpendicular to the fiber axis), the polarization direction relative to the fiber axis has an important influence on the SHG emission power.

3.2 *Effects of the Numerical Aperture (NA) on SHG Emission*

The most important parameter to characterize the focused beam is the numerical aperture, NA=$n_\omega \sin\phi$, where ϕ represents the incident angle of the illumination light (please refer to Fig. 1).

The focus of the light causes the phase retardation near the focus center along the axial direction. This phase retardation is called Guoy phase shift and can be represented by a wave-vector reduction factor ξ. The change of NA will induce the change of ξ as approximately by $\xi \approx \cos(\phi/\sqrt{2})$ (when NA$<$1.2 at most[8]).

In our single-fibril model, the phase match term, including the Guoy phase shift and the dispersion due to the refraction index change between the incident (n_ω) and second harmonic frequency $(n_{2\omega})$, can be expressed as

$$\Delta\vec{k} = \vec{k}_{2\omega} - 2\xi\vec{k}_\omega (k_\omega = 2\pi n_\omega/\lambda_\omega \text{ and } k_{2\omega} = 2\pi n_{2\omega}/\lambda_{2\omega}). \tag{20}$$

ξ appears in the axial direction of the focal ellipse (w_z) exclusively. Momentum conservation along the axial direction then forces the SHG $(k_{2\omega})$ to propagate at an off-axis angle θ. This angle θ is $\theta=\cos^{-1}[\xi(n_\omega/n_{2\omega})]$ to satisfy the phase-match condition, $k_{2\omega}\cos\theta - 2\xi k_\omega = 0$, thus achieves the max SHG emission intensity. Figure 4(a) illustrates the relationship between the phase match terms. The solid arrow stands for the condition of phase match, and the dash arrow represents for condition of the phase mismatch. $\xi' = \xi n_\omega/n_{2\omega}$ has been introduced in Eq. (33c) in Appendix B thus $\theta=\cos^{-1}(\xi)$. If $n_\omega = n_{2\omega}$, where dispersion effect has been ignored, then $\theta = \cos^{-1}(\xi)$.

In this paper, the refractive index of SHG and fundamental excitation light in collagen are correspondingly taken to be $n_{2\omega}$=1.503, n_ω=1.453 based on the research results from Bashkatov et al..[20] To demonstrate the influence of NA under the consideration of dispersion, SHG emissions under NA=0.8 and NA=0.2 has been compared as those shown in Fig. 4(b). We note that due to the influence of dispersion, no matter at high NA or low NA, SHG emission presents two off-axis lobes. However, at higher NA, the SHG emission lobes are much more distributed and detached, the max value of SHG emission appears at the angle of θ=27 deg. On the other hand, at lower NA, the SHG emission concentrates along small angle θ=16 deg and has much weaker intensity.

To investigate how NA under polarized beam influences the total power, parallel, and perpendicular components, $P_{2\omega}$, $P_{2\omega}^{\parallel}$, and $P_{2\omega}^{\perp}$ [all data are normalized by $(1/8)n_{2\omega}\varepsilon_0 c\,\eta^2 N^2 E_\omega^{(0)4}=1$] along NA, which vary from 0–1.0 under polarization angle α=0,30,60,90 deg is demonstrated in Fig. 5. In general, we note that the total emission power of SHG increases as the increase of NA, but the change does not show linearity. As the increase of NA, SHG parallel emission at α=0,30,60 deg has the similar trend of change but different degree and at α=90 deg, there is no change. Whereas SHG perpendicular emission also increases at different degree when α=30,60,90 deg and the slight increase at α=0 deg can be ignored. As the polarization angle α changes from 0 to 90 deg, the total and parallel components of SHG emission power decrease, while the perpendicular one increases.

3.3 *Effects of the Ratio $\rho=\beta_{xxx}/\beta_{xyy}$ under Different Polarization Direction*

β is the hyperpolarizability of the collagen fibrils which is related to the electronic transition in the material, thus reflects its biological structure and chemical features.[21,22] In our specific collagen model with the polarized illumination beam,

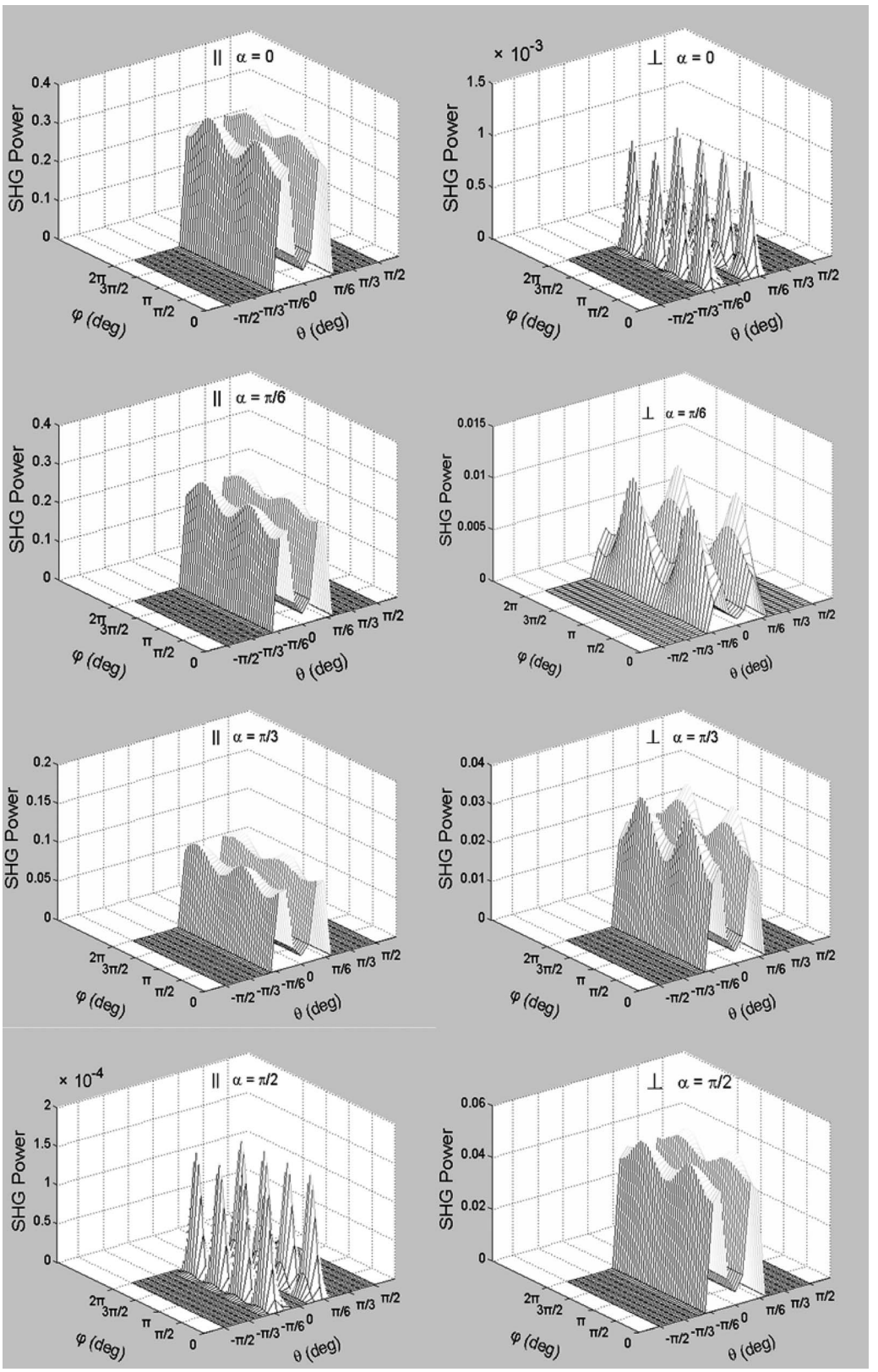

Fig. 3 Effects of polarization angle α on SHG emission power distribution (θ, φ) of parallel $P_{2\omega}^{\parallel}$ and perpendicular $P_{2\omega}^{\perp}$ components.

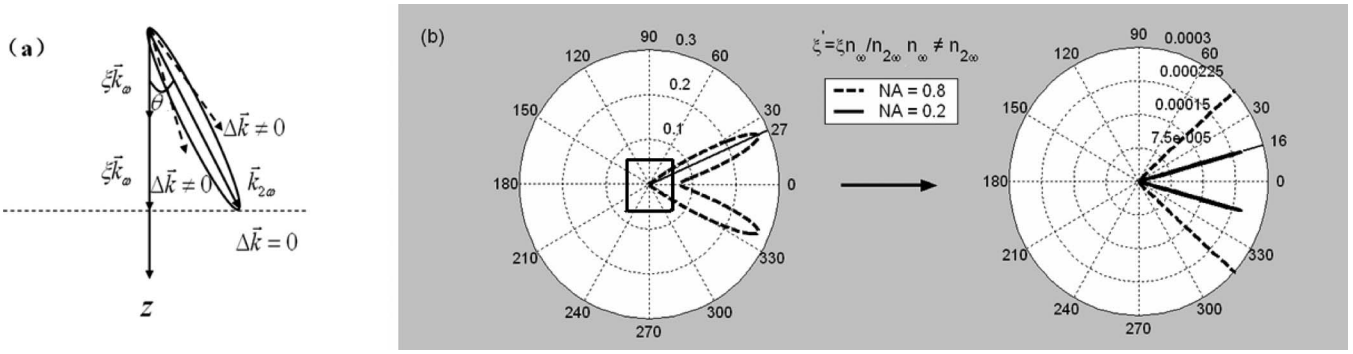

Fig. 4 Phase-match condition makes SHG propagate in the direction of $k_{2\omega}$, which deviates an angle of θ with respect to incident beam k_ω due to the Guoy phase shift (ξ) and dispersion. (b) Effects of NA on SHG electrical radiation pattern (on the right is the enlargement part from the square center of the image on the left).

two elements β_{xxx}, β_{xyy} remain and have the contribution to SHG. The ratio $\rho=\beta_{xxx}/\beta_{xyy}$ plays very important role in characterizing the collagen features. It has been proved that ρ increases with the increasing of age.[9,11] As mentioned above, $\rho=\beta_{xxx}/\beta_{xyy}$ has been predicted to vary between −3 to 3.[19] The minus value of ρ suggests the polarity of the fibrils reverse from the excited electrical field. The study of the effect of ρ on SHG emission power may provide us significant information for tissue characterization.

How the value of $\rho=\beta_{xxx}/\beta_{xyy}$ varies from −3 to 3 influence the total power, parallel and perpendicular components at different polarization angle α has been three-dimensionally presented in Fig. 6. The overall configuration of the SHG emission pattern indicates that the influence of minus value and positive value of ρ is not symmetric when $\alpha\neq 0$ deg. For more details, two-dimensional figures under four particular polarization angles $\alpha=0,30,60,90$ deg are selectively demonstrated in Fig. 7. We note that no matter the total, parallel or the perpendicular components, at different polarization conditions, the change patterns as ρ are quite different. And from minus value to positive value of ρ, the change patterns are not symmetric except under the excitation condition of $\alpha=0$ deg. At polarization angle $\alpha=90$ deg, different ρ makes $P_{2\omega}$, $P_{2\omega}^{\parallel}$, and $P_{2\omega}^{\perp}$ have no change. At polarization $\alpha=0$ deg, as the absolute value of ρ increases, all SHG emission power (total, parallel, and perpendicular components) increases; however, the increase; of ρ has minor contribution to the perpendicular one. At polarization $\alpha=30$ deg, as ρ changes from −3 to 3, the total, parallel, and perpendicular components of the SHG emission power change from high to low value and then increase again, but the lowest turning point does not locate at $\rho=0$. At polarization $\alpha=60$ deg, the curves increase slowing and have no obvious turning point along ρ except in the perpendicular one, which slightly shows a turning.

4 Discussion and Conclusions

In this paper, a theoretical model of SHG on type I collagen under polarized focused beam has been established. On the basis of this model, we have investigated the total, parallel, perpendicular SHG emission power and their distribution along (θ,φ), induced by different polarization angles α of the illumination light. The total, parallel, and perpendicular SHG emission power periodically change as the polarization angle α, similar to the pattern produced from the uniformly distributed dye dipoles on the cell membrane. The distribution of parallel, perpendicular components along (θ,φ) is complicated and possesses multiple peaks, but they symmetrically distribute around the plane, where fibrils locate ($\theta=0$ deg, $\varphi=180$ deg). NA is another important factor that influences the illumination source. Therefore, the effects of NA on SHG emission are also investigated. At lower NA (for example, NA=0.2), the SHG emission concentrates in two closer lobes (like two lines), while at relative higher NA, such as NA =0.8, SHG emission pattern has changed to be two obvious

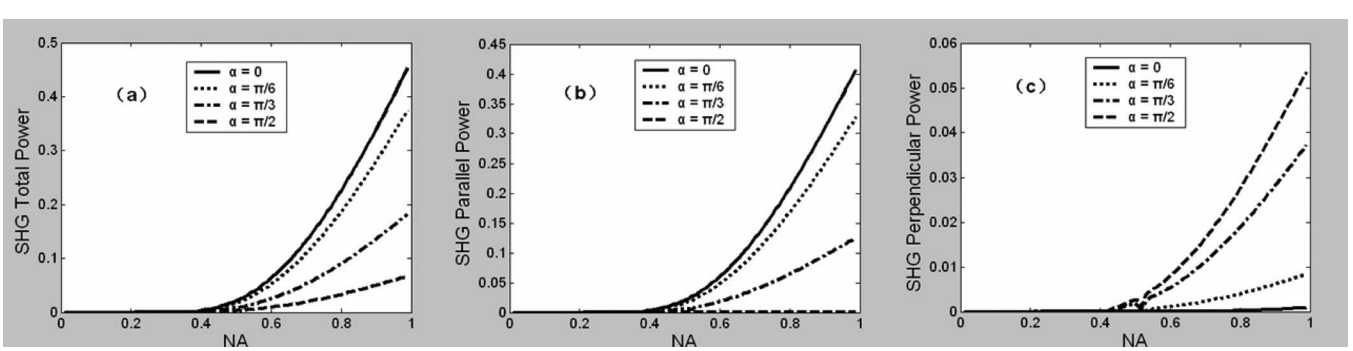

Fig. 5 Effects of NA on total $P_{2\omega}$, parallel $P_{2\omega}^{\parallel}$, and perpendicular $P_{2\omega}^{\perp}$ components of SHG emission power under different polarization angle α.

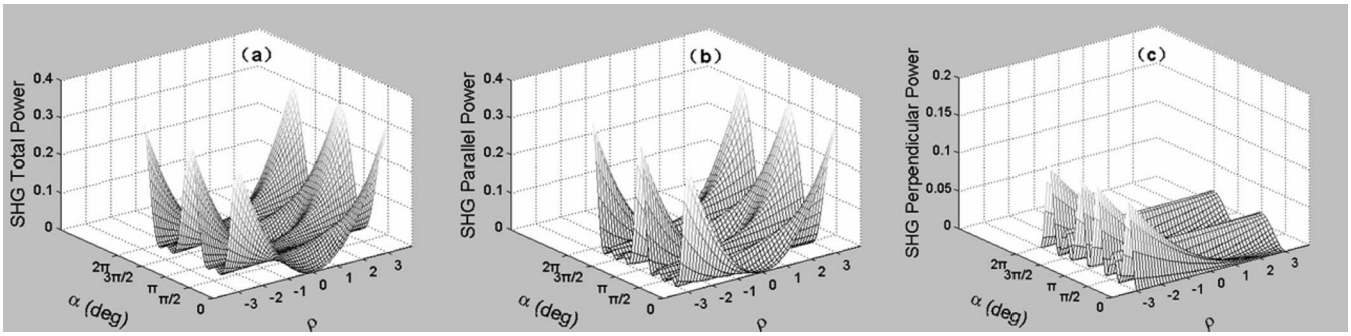

Fig. 6 Three-dimensional demonstration of effects of ratio ρ of hyperpolarizability elements of β_{xxx} to β_{xyy} on total, parallel, and perpendicular SHG power emission at different polarization angle α.

distributed lobes. At lower NA, where the light is loosely focused, it acts like a collimated light on the samples; thus, the influence from the Guoy phase shift can be ignored and dispersion alone plays role on SHG emission. According to $\theta=\cos^{-1}[\xi(n_\omega/n_{2\omega})]$, when $\xi=1$ (unfocused light by very low NA), the emission angle θ is smaller than that at $\xi<1$ (focused light by high NA). However, at relative higher NA, where the light is tightly focused, because of the Guoy shift (phase shift) induced by focusing as well as the dispersion effect, to keep the momentum equilibrium, SHG emission strays far away from the direction of illumination light. As NA increases, we realizes that the waists of w_{xy} and w_z decreases. On the basis of expression A in Eq. (12), we understand that NA not only affects the emission angle θ, but also the distribution of the emission. At higher NA, SHG emission is much more distributed. The combination effect of NA under different polarization angles α is also studied. We find the influence of NA on SHG emission under different excitation conditions of polarization angle α is different, and the contribution of different NA to SHG emission is not linearity. However, our theoretical analysis results of NA are not applicable for linearly polarized light being focused with an objective with very high NA, because under such conditions, the polarization is no longer constant within the focus volume. At last, the ratio ρ of two existing components of β, which are β_{xxx} and β_{xyy} in our case is explored. Twenty-seven items of β are reduced to seven nonzero elements (two independent) through cylindrical symmetry and rule of Kleinman symmetry. For the light linearly polarized in x-y plane ($\varepsilon_z=0$), those leave only two elements β_{xxx} and β_{xyy}. Here, the inconsistency of the polarization angle α with respect to the fiber axis keeps one more valid hyperpolarizability element β_{xyy} of collagen in the model rather than β_{xxx} alone at $\alpha=0$ deg. As we have mentioned in Sec. 3.3, the significance of ρ to collagen is obvious; therefore, SHG emission study of the changes of ρ may offers us important clues of the relationship between SHG emission with collagen features, such as its maturity, polarity, as well as the pathologically induced characterization changes.

In conclusion, our theoretical simulation results provide useful clues for experimental study of microscopic SHG in collagen type I under linearly polarized beam.

Acknowledgment

The authors gratefully thank the National Natural Science Foundation of China (Grant No: 30470495) for its support.

Appendix A: Simplification of Nonlinear Optical Hyperpolarizability

$\vec{\mu}_{2\omega,i}(x,y,z)$ has three components, which are in the x, y, and z directions respectively,

$$\vec{\mu}_{2\omega,i}(x,y,z)=\frac{1}{2}\vec{E}^2_\omega(x,y,z)\sum_{j,k}\langle\beta_{ijk}\rangle\hat{\varepsilon}_j\hat{\varepsilon}_k. \tag{21}$$

Its subscript i presents these three directions. On the basis of the definition of the second-order tensor, hyperpolarizabilities β owns 27 items

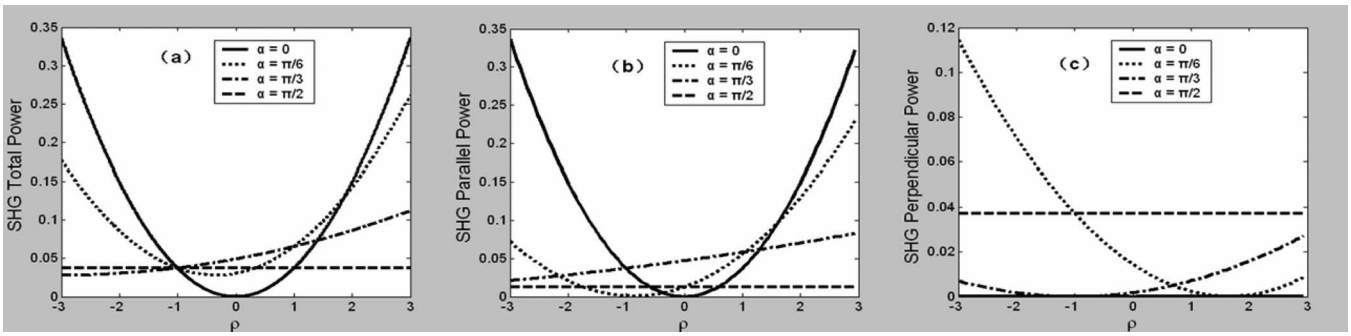

Fig. 7 Two-dimensional demonstration of effects of ratio ρ of hyperpolarizability elements of β_{xxx} to β_{xyy} on total, parallel, and perpendicular SHG power emission at different polarization angle α.

$$\begin{pmatrix} \beta_{xxx} & \beta_{xyy} & \beta_{xzz} & \beta_{xyz} & \beta_{xzy} & \beta_{xzx} & \beta_{xxz} & \beta_{xxy} & \beta_{xyx} \\ \beta_{yxx} & \beta_{yyy} & \beta_{yzz} & \beta_{yyz} & \beta_{yzy} & \beta_{yzx} & \beta_{yxz} & \beta_{yxy} & \beta_{yyx} \\ \beta_{zxx} & \beta_{zyy} & \beta_{zzz} & \beta_{zyz} & \beta_{zzy} & \beta_{zzx} & \beta_{zxz} & \beta_{zxy} & \beta_{zyx} \end{pmatrix}. \tag{22}$$

A.1 Kleinman Symmetry

The assumption of Kleinman symmetry condition is applied to lossless media.[23] It is valid if the frequency ω of excitation light is far from any natural frequencies of material. Because near-infrared light is usually used for SHG in biological tissue, in our case, if light with 800-nm wavelength is assumed to be used, then it is far from the wavelength of the first electronic transition in collagen ($\sim$310 nm),[24] and therefore, Kleinman symmetry applies. Within in the validity of Kleinman symmetry,[25–28]

$$\beta_{ijk} = \beta_{jki} = \beta_{kij} = \beta_{ikj} = \beta_{jik} = \beta_{kji}. \tag{23}$$

As a result, only ten independent elements of β remain, which are as follows:

$$xxx, yyy, zzz, xyy = yxy = yyx, \quad xzz = zxz = zzx, \quad xxy = xyx = yxx,$$

$$xxz = xzx = zxx, \quad yzz = zyz = zzy, \quad zyy = yzy = yyz, \quad xyz = xzy = yxz = yzx = zxy = zyx. \tag{24}$$

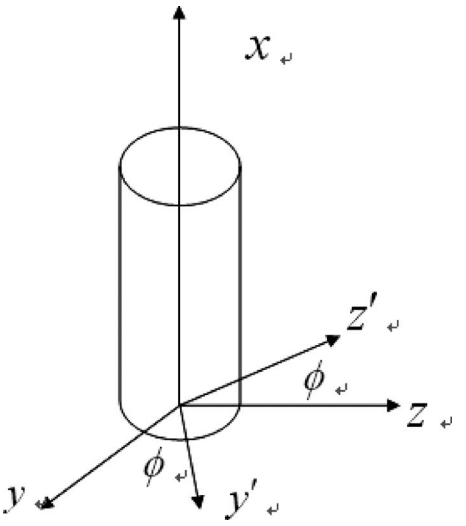

Fig. 8 Schematic diagram of cylindrical symmetry of collagen fiber along $\vec{x}$-axis.

A.2 Cylindrical Symmetry

Collagen fiber possesses cylindrically symmetrical feature in structure[29–31] (as shown in Fig. 8). Under such condition, the hyperpolarizability tensor can be further simplified. The cylinder symmetry indicates that by taking the changes of $x \rightarrow x$, $y \rightarrow -y$, $z \rightarrow -z$ on the subscripts of matrix β_{ijk} in Eq. (22), the derived new matrix of β_{ijk} in Eq. (5) should be the same as those in Eq. (22)

$$\begin{pmatrix} xxx & xyy & xzz & xyz & xzy & -xzx & -xxz & -xxy & -xyx \\ -yxx & -yyy & -yzz & -yyz & -yzy & yzx & yxz & yxy & yyx \\ -zxx & -zyy & -zzz & -zyz & -zzy & zzx & zxz & zxy & zyx \end{pmatrix}. \tag{25}$$

Therefore, the elements in Eq. (25) with minus sign should be zero and the elements of β now become

$$\begin{pmatrix} xxx & xyy & xzz & xyz & xzy & 0 & 0 & 0 & 0 \\ 0 & 0 & 0 & 0 & 0 & yzx & yxz & yxy & yyx \\ 0 & 0 & 0 & 0 & 0 & zzx & zxz & zxy & zyx \end{pmatrix}. \tag{26}$$

Also, from Fig. 8, we get the relation between y and z because the cylinder symmetry by applying $x \rightarrow x$, $y \rightarrow y'$, $z \rightarrow z'$

$$x = x, \quad y = y' \cos\phi - z' \sin\phi, \quad z = y' \sin\phi + z' \cos\phi. \tag{27}$$

A project matrix is used to present the relationship.

$$\begin{pmatrix} x \\ y \\ z \end{pmatrix} = \begin{pmatrix} 1 & 0 & 0 \\ 0 & \cos\phi & -\sin\phi \\ 0 & \sin\phi & \cos\phi \end{pmatrix} \begin{pmatrix} x' \\ y' \\ z' \end{pmatrix} = \begin{pmatrix} l_{xx} & l_{xy} & l_{xz} \\ l_{yx} & l_{yy} & l_{yz} \\ l_{zx} & l_{zy} & l_{zz} \end{pmatrix} \begin{pmatrix} x' \\ y' \\ z' \end{pmatrix}. \tag{28}$$

Or, further to be

$$\beta_{ijk} = l_{ii'} l_{jj'} l_{kk'} \beta_{i'j'k'}. \tag{29}$$

According to the above expression, we have the following relationship:

$$\beta_{xxx} = l_{xx'} l_{xx'} l_{xx'} \beta_{x'x'x'}, \quad \beta_{xyy} = l_{xx} l_{yz} l_{yz} \beta_{xzz} = \sin^2\phi \beta_{xzz},$$

$$\beta_{xyz} = l_{xx} l_{yz} l_{zy} \beta_{xzy} = -\sin^2\phi \beta_{xzy}, \quad \beta_{yyx} = l_{yz} l_{yz} l_{xx} \chi_{zzx} = \sin^2\phi \beta_{zzx}$$

$$\beta_{yxy} = l_{yz}l_{xx}l_{yz}\beta_{zxz} = \sin^2\phi\beta_{zxz}, \quad \beta_{yzx} = l_{yz}l_{zy}l_{xx}\chi_{zyx} = -\sin^2\phi\beta_{zyx}$$

$$\beta_{yxz} = l_{yz}l_{xx}l_{zy}\chi_{zxy} = -\sin^2\phi\beta_{zxy}$$

The rotation between y and z, ϕ=90 or 270 deg, makes $\sin^2\phi$=1. Accoding to Eq. (4), we get

$$\beta_{xxx}, \tag{30a}$$

$$\beta_{xyy} = \beta_{xzz} = \beta_{yyx} = \beta_{zzx} = \beta_{yxy} = \beta_{zxz}, \tag{30b}$$

$$\beta_{xyz} = \beta_{xzy} = \beta_{yxz} = \beta_{yzx} = \beta_{zxy} = \beta_{zyx} = 0. \tag{30c}$$

As a result, there are only seven nonzero elements, in particular, two independent elements.

In our case, for the light linearly polarized in $x-y$ plane ($\vec{E}_\omega$), ε_z=0. It remains only two (β_{xxx}, β_{xyy}) of the above seven nonzero elements has the contribution to the dipole moment μ, thus to the SHG emission.

Appendix B: Integration of SHG emission electric field

In this part, we demonstrate the integration of the SHG emission electric field in x, y, z direction from negative infinite to positive infinite.

$$\begin{aligned}\vec{E}_{2\omega}(\theta,\varphi) = \frac{\eta N_V}{r}\int\int\int \sin\psi\cdot\vec{\mu}_{2\omega}(x,y,z)\exp[&\\ -ik_{2\omega}(z\cos\theta + y\sin\theta\sin\varphi &\\ + x\sin\theta\cos\varphi)]dxdydz = \eta N_V/r(\sin^2\theta\sin^2\varphi &\\ + \cos^2\theta)^{1/2}\int\int\int\cdot\frac{1}{2}\beta\vec{E}_\omega^{(0)2}\exp\left(-2\frac{x^2+y^2}{w_{xy}^2}\right.&\\ \left.-2\frac{z^2}{w_z}+2i\xi k_\omega z\right)\times\exp[-ik_{2\omega}(z\cos\theta &\\ + y\sin\theta\sin\varphi + x\sin\theta\cos\varphi)]dxdydz &\\ = N_V\frac{\eta}{r}(\sin^2\theta\sin^2\varphi+\cos^2\theta)^{1/2}\cdot\vec{\mu}_{2\omega}^{(0)}&\end{aligned} \tag{31a}$$

$$\times\int\exp\left(-\frac{2x^2}{w_{xy}^2}-ik_{2\omega}x\sin\theta\cos\varphi\right)dx \tag{31b}$$

$$\times\int\exp\left(-\frac{2y^2}{w_{xy}^2}-ik_{2\omega}y\sin\theta\sin\varphi\right)dy \tag{31c}$$

$$\times\int\exp\left(-\frac{2z^2}{w_z^2}+2i\xi k_\omega z-ik_{2\omega}z\cos\theta\right)dz. \tag{31d}$$

According to the following integral equation,

$$\int_{-\infty}^{+\infty}\exp(-p^2x^2\pm qx)dx = \exp\left(\frac{q^2}{4p^2}\right)\frac{\sqrt{\pi}}{p} \quad (\mathrm{Re}\,p^2>0) \tag{32}$$

Equations (31b)–(31d) have the corresponding parameters of p and q, such as

$$p^2 = \frac{2}{w_{xy}^2}, \quad p = \frac{\sqrt{2}}{w_{xy}}, \quad q = ik_{2\omega}\sin\theta\cos\varphi, \quad q^2 = -k_{2\omega}^2(\sin\theta\cos\varphi)^2$$

$$\int\exp\left(-\frac{2x^2}{w_{xy}^2}-ik_{2\omega}x\sin\theta\cos\varphi\right)dx = \exp\left[-\frac{k_{2\omega}^2}{8}w_{xy}^2(\sin\theta\cos\varphi)^2\right]\sqrt{\frac{\pi}{2}}w_{xy} \tag{33a}$$

$$p^2 = \frac{2}{w_{xy}^2}, \quad p = \frac{\sqrt{2}}{w_{xy}}, \quad q = ik_{2\omega}\sin\theta\sin\varphi, \quad q^2 = -k_{2\omega}^2(\sin\theta\sin\varphi)^2$$

$$\int\exp\left(-\frac{2y^2}{w_{xy}^2}-ik_{2\omega}y\sin\theta\sin\varphi\right)dy = \exp\left[-\frac{k_{2\omega}^2}{8}w_{xy}^2(\sin\theta\sin\varphi)^2\right]\sqrt{\frac{\pi}{2}}w_{xy} \tag{33b}$$

$$p^2 = \frac{2}{w_z^2}, \quad p = \frac{\sqrt{2}}{w_z}, \quad q = ik_{2\omega}\cos\theta - 2i\xi k_\omega$$

$$k_\omega = \frac{2\pi n_\omega}{\lambda_\omega}, \quad k_{2\omega} = \frac{2\pi n_{2\omega}}{\lambda_{2\omega}}, \quad \xi' = \xi\frac{n_\omega}{n_{2\omega}},$$

$$q^2 = -k_{2\omega}^2(\cos\theta-\xi')^2$$

$$\int\exp\left(-\frac{2z^2}{w_z^2}+2i\xi k_\omega z-ik_{2\omega}z\cos\theta\right)dz = \exp\left[-\frac{k_{2\omega}^2}{8}w_z^2(\cos\theta-\xi')^2\right]\sqrt{\frac{\pi}{2}}w_z. \tag{33c}$$

Appendix C: Total Power of SHG

The relation between total power distribution of SHG and electric field is[18]

$$P_{2\omega}(\theta,\varphi)=\frac{1}{2}n_{2\omega}\varepsilon_0 c r^2 E_{2\omega}^2(\theta,\varphi)$$
$$=\frac{1}{2}n_{2\omega}\varepsilon_0 c r^2 N^2 A^2(\theta,\varphi)E_{2\omega}^{(0)2}(\theta,\varphi)$$
$$=\frac{1}{2}n_{2\omega}\varepsilon_0 c r^2 N^2 A^2(\theta,\varphi)\frac{\eta^2}{r^2}(\sin^2\theta\sin^2\varphi+\cos^2\theta)\mu_{2\omega}^{(0)2}$$
$$=\frac{1}{8}n_{2\omega}\varepsilon_0 c\,\eta^2 N^2 A^2(\theta,\varphi)E_{\omega}^{(0)4}(\sin^2\theta\sin^2\varphi+\cos^2\theta)\beta^2=\frac{1}{8}n_{2\omega}\varepsilon_0 c\,\eta^2 N^2 E_{\omega}^{(0)4}A^2(\theta,\varphi)(1-\sin^2\theta\cos^2\varphi)\begin{pmatrix}\beta_{xxx}\cos^2\alpha+\beta_{xyy}\sin^2\alpha\\ \beta_{xyy}\sin 2\alpha\\ 0\end{pmatrix}^2. \quad (34)$$

The total power of SHG then is derived from double integral on θ and φ in a solid angle,

$$P_{2\omega}=\int\int P_{2\omega}(\theta,\varphi)\sin\theta d\theta d\varphi$$
$$=\int\int\frac{1}{2}n_{2\omega}\varepsilon_0 c r^2 N^2 A^2(\theta,\varphi)\frac{\eta^2}{r^2}(\sin^2\theta\sin^2\varphi+\cos^2\theta)\mu_{2\omega}^{(0)2}\sin\theta d\theta d\varphi=\frac{1}{2}n_{2\omega}\varepsilon_0 c\,\eta^2 N^2\int\int A^2(\theta,\varphi)\times(\sin^2\theta\sin^2\varphi+\cos^2\theta)\mu_{2\omega}^{(0)2}\sin\theta d\theta d\varphi$$
$$=\frac{1}{2}n_{2\omega}\varepsilon_0 c\,\eta^2 N^2\Theta(\mu_{2\omega,x}^{(0)2}+\mu_{2\omega,y}^{(0)2}+\mu_{2\omega,z}^{(0)2})$$
$$=\frac{1}{8}n_{2\omega}\varepsilon_0 c\,\eta^2 N^2\Theta E_{\omega}^{(0)4}[(\beta_{xxx}\cos^2\alpha+\beta_{xyy}\sin^2\alpha)^2+(\beta_{xyy}\sin 2\alpha)^2].$$

$$\Theta=\int\int A^2(\theta,\varphi)(1-\sin^2\theta\cos^2\varphi)\sin\theta d\theta d\varphi$$

$$\vec{\mu}_{2\omega}^{(0)}=\begin{pmatrix}\mu_{2\omega,x}^{(0)}\\ \mu_{2\omega,y}^{(0)}\\ \mu_{2\omega,z}^{(0)}\end{pmatrix}=\frac{1}{2}\vec{E}_{\omega}^{(0)2}\begin{pmatrix}\beta_{xxx}\cos^2\alpha+\beta_{xyy}\sin^2\alpha\\ \beta_{xyy}\sin 2\alpha\\ 0\end{pmatrix}. \quad (35)$$

Appendix D: Parallel and Perpendicular Components of SHG Emission Power

$$\begin{pmatrix}E_{2\omega}^{\parallel}\\ E_{2\omega}^{\perp}\end{pmatrix}=\begin{bmatrix}\cos(\varphi-\alpha) & -\sin(\varphi-\alpha)\\ \sin(\varphi-\alpha) & \cos(\varphi-\alpha)\end{bmatrix}\begin{pmatrix}E_{2\omega}^{p}\\ E_{2\omega}^{s}\end{pmatrix},$$

$$E_{2\omega}^{\parallel}=E_{2\omega}^{p}\cos(\varphi-\alpha)-E_{2\omega}^{s}\sin(\varphi-\alpha),$$

$$E_{2\omega}^{\perp}=E_{2\omega}^{p}\sin(\varphi-\alpha)+E_{2\omega}^{s}\cos(\varphi-\alpha).$$

The parallel and perpendicular SHG emission power distributions are

$$P_{2\omega}^{\parallel}(\theta,\varphi)=\frac{1}{2}n_{2\omega}\varepsilon_0 c r^2|E_{2\omega}^{\parallel}(\theta,\varphi)|^2=\frac{1}{2}n_{2\omega}\varepsilon_0 c r^2[\cos(\varphi-\alpha)E_{2\omega}^{p}-\sin(\varphi-\alpha)E_{2\omega}^{s}]^2, \quad (36a)$$

$$P_{2\omega}^{\perp}(\theta,\varphi)=\frac{1}{2}n_{2\omega}\varepsilon_0 c r^2|E_{2\omega}^{\perp}(\theta,\varphi)|^2=\frac{1}{2}n_{2\omega}\varepsilon_0 c r^2[\sin(\varphi-\alpha)E_{2\omega}^{p}+\cos(\varphi-\alpha)E_{2\omega}^{s}]^2. \quad (36b)$$

While

$$\vec{E}_{2\omega}^{(0)}(\theta,\varphi)=\begin{pmatrix}E_{2\omega}^{(0),p}(\theta,\varphi)\\ E_{2\omega}^{(0),s}(\theta,\varphi)\end{pmatrix}=\frac{\eta}{r}\vec{M}\cdot\vec{\mu}_{2\omega}^{(0)}=\frac{\eta}{r}\vec{M}\cdot\frac{1}{2}\vec{E}_{\omega}^{(0)2}\beta=\frac{\eta}{2r}E_{\omega}^{(0)2}\begin{pmatrix}\cos\theta\cos\varphi & \cos\theta\sin\varphi & -\sin\theta\\ -\sin\varphi & \cos\varphi & 0\end{pmatrix}\begin{pmatrix}\beta_{xxx}\cos^2\alpha+\beta_{xyy}\sin^2\alpha\\ \beta_{xyy}\sin 2\alpha\\ 0\end{pmatrix}$$
$$=\frac{\eta}{2r}E_{\omega}^{(0)2}\begin{pmatrix}\cos\theta\cos\varphi(\beta_{xxx}\cos^2\alpha+\beta_{xyy}\sin^2\alpha)+\beta_{xyy}\cos\theta\sin\varphi\sin 2\alpha\\ -\sin\varphi(\beta_{xxx}\cos^2\alpha+\beta_{xyy}\sin^2\alpha)+\beta_{xyy}\cos\varphi\sin 2\alpha\end{pmatrix}.$$

Therefore,

$$E_{2\omega}^{(0),p}(\theta,\varphi)=\frac{\eta}{2r}E_{\omega}^{(0)2}[\cos\theta\cos\varphi(\beta_{xxx}\cos^2\alpha+\beta_{xyy}\sin^2\alpha)+\beta_{xyy}\cos\theta\sin\varphi\sin 2\alpha],$$

$$E_{2\omega}^{(0),s}(\theta,\varphi)=\frac{\eta}{2r}E_{\omega}^{(0)2}[-\sin\varphi(\beta_{xxx}\cos^2\alpha+\beta_{xyy}\sin^2\alpha)+\beta_{xyy}\cos\varphi\sin 2\alpha],$$

$$E_{2\omega}(\theta,\varphi)=NE_{2\omega}^{(0)}A(\theta,\varphi)=\frac{\eta NA(\theta,\varphi)}{2r}E_{\omega}^{(0)2}\begin{pmatrix}\cos\theta\cos\varphi(\beta_{xxx}\cos^2\alpha+\beta_{xyy}\sin^2\alpha)+\beta_{xyy}\cos\theta\sin\varphi\sin 2\alpha\\ -\sin\varphi(\beta_{xxx}\cos^2\alpha+\beta_{xyy}\sin^2\alpha)+\beta_{xyy}\cos\varphi\sin 2\alpha\end{pmatrix},$$

$$E_{2\omega}^{p}(\theta,\varphi)=\frac{\eta NA(\theta,\varphi)}{2r}E_{\omega}^{(0)2}[\cos\theta\cos\varphi(\beta_{xxx}\cos^2\alpha+\beta_{xyy}\sin^2\alpha)+\beta_{xyy}\cos\theta\sin\varphi\sin 2\alpha],$$

$$E_{2\omega}^{s}(\theta,\varphi)=\frac{\eta NA(\theta,\varphi)}{2r}E_{\omega}^{(0)2}[-\sin\varphi(\beta_{xxx}\cos^2\alpha+\beta_{xyy}\sin^2\alpha)+\beta_{xyy}\cos\varphi\sin 2\alpha].$$

At last,

$$P_{2\omega}^{\parallel}(\theta,\varphi)=\frac{1}{8}n_{2\omega}\varepsilon_0 c\,\eta^2N^2A^2(\theta,\varphi)E_{\omega}^{(0)4}\{\cos(\varphi-\alpha)\times[\cos\theta\cos\varphi(\beta_{xxx}\cos^2\alpha+\beta_{xyy}\sin^2\alpha)+\beta_{xyy}\cos\theta\sin\varphi\sin 2\alpha]-\sin(\varphi-\alpha)\times[-\sin\varphi(\beta_{xxx}\cos^2\alpha+\beta_{xyy}\sin^2\alpha)+\beta_{xyy}\cos\varphi\sin 2\alpha]\}^2. \quad (37a)$$

$$P_{2\omega}^{\perp}(\theta,\varphi)=\frac{1}{8}n_{2\omega}\varepsilon_0 c\,\eta^2N^2A^2(\theta,\varphi)E_{\omega}^{(0)4}\{\sin(\varphi-\alpha)\times[\cos\theta\cos\varphi(\beta_{xxx}\cos^2\alpha+\beta_{xyy}\sin^2\alpha)+\beta_{xyy}\cos\theta\sin\varphi\sin 2\alpha]+\cos(\varphi-\alpha)\times[-\sin\varphi(\beta_{xxx}\cos^2\alpha+\beta_{xyy}\sin^2\alpha)+\beta_{xyy}\cos\varphi\sin 2\alpha]\}^2. \quad (37b)$$

References

1. W. R. Zipfel, R. M. Williams, and W. W. Webb, "Nonlinear magic: multiphoton microscopy in the biosciences," *Nat. Biotechnol.* **21**(11), 1368–1376 (2003).
2. F. Helmchen and W. Denk, "Deep tissue two-photon microscopy," *Nat. Methods* **2**(12), 932–940 (2005).
3. E. Brown, T. McKee, E. diTomaso, A. Pluen, B. Seed, Y. Boucher, and R. K. Jain, "Dynamic imaging of collagen and its modulation in tumors *in vivo* using second-harmonic generation," *Nat. Methods* **9**(6), 796–800 (2003).
4. G. Cox, E. Kable, A. Jones, I. Fraser, F. Manconi, and M. D. Gorrell, "3-Dimensional imaging of collagen using second harmonic generation," *J. Struct. Biol.* **141**, 53–62 (2003).
5. D. J. Prockop and A. Fertala, "The collagen fibril: the almost crystalline structure," *J. Struct. Biol.* **122**, 111–118 (1998).
6. K. Beck and B. Brodsky, "Supercoiled protein motifs: the collagen triple-helix and the helical coiled coil," *J. Struct. Biol.* **122**, 17–29 (1998).
7. I. Freund and M. Deutsch, "Second-harmonic microscopy of biological tissue," *Opt. Lett.* **11**, 94–96 (1986).
8. L. Moreaux, O. Sandre, and J. Mertz, "Membrane imaging by second-harmonic generation microscopy," *J. Opt. Soc. Am. B* **17**, 168–1694 (2000).
9. S. Roth and I. Freund, "Second harmonic generation in collagen," *J. Chem. Phys.* **70**(4), 1637–1643 (1979).
10. I. Freund, M. Deutsch, and A. Sprecher, "Connective tissue polarity optical second-harmonic microscopy, crossed-beam summation, and small-angle scattering in rat-tail tendon," *Biophys. J.* **50**, 693–712 (1986).
11. R. M. Williams, W. R. Zipfel, and W. W. Webb, "Interpreting second harmonic generation images of collagen I fibrils," *Biophys. J.* **80**(2), 1377–1386 (2005).
12. P. J. Campagnola, M.-d. Wei, A. Lewis, and L. M. Loew, "High-resolution nonlinear optical imaging of live cells by second harmonic generation," *Biophys. J.* **77**, 3341–3349 (1999).
13. R. Gauderon, P. B. Lukins, and C. J. R. Sheppard, "Simultaneous multichannel nonlinear imaging: combined two-photon excited fluorescence and second-harmonic generation microscopy," *Micron* **32**, 685–689 (2001).
14. P. J. Campagnola and L. M. Loew, "Second-harmonic imaging microscopy for visualizing biomolecular arrays in cells, tissues and organisms," *Nature (London)* **21**(11), 1356–1360 (2003).
15. J. E. Bjorkholm, "Optical second-harmonic generation using a focused Gaussian laser beam," *Phys. Rev.* **142**(1), 126–136 (1966).
16. A. Willetts, J. E. Rice, and D. M. Burland, "Problems in the comparison of theoretical and experimental hyperpolarizabilities," *J. Chem. Phys.* **97**(10), 7590–7599 (1992).
17. E. Hecht, *Optics*, Higher Education Press, Beijing (2005).
18. J. Mertz and L. Moreaux, "Second-harmonic generation by focused excitation of inhomogeneously distributed scatterers," *Opt. Commun.* **196**, 325–330 (2001).
19. C. Odin, Y. L. Grand, A. Renault, L. Gailhouste, and G. Baffet, "Orientation fields of nonlinear biological fibrils by second harmonic generation microscopy," *J. Microsc.* **229**, 32–38 (2008).
20. A. N. Bashkatov, E. A. Genina, V. I. Kochubey, and V. V. Tuchin, "Estimation of wavelength dependence of refractive index of collagen fibers of scleral tissue," *Proc. SPIE* **4162**, 265–268 (2000).
21. S.-W. Chu, S.-Y. Chen, G.-W. Cher, T.-H. Tsai, Y.-C. Chen, B.-L. Lin, and C.-K. Sun, "Studies of $x(2)/x(3)$ tensors in submicron-scaled bio-tissues by polarization harmonics optical microscopy," *Biophys. J.* **86**, 3914–3922 (2004).
22. Y. Fu, H. Wang, R. Shi, and J. X. Cheng, "Second harmonic and sum frequency generation imaging of fibrous astroglial filaments in ex vivo spinal tissues," *Biophys. J.* **92**, 3251–3259 (2007).
23. R. W. Boyd, *Nonlinear optics*, Academic Press (1992).
24. P. Stoller, K. M. Reiser, P. M. Celliers, and A. M. Rubenchik., "Polarization-modulated second harmonic generation in collagen. Biophys," *Biophys. J.* **82**, 3330–3342 (2002).
25. K. A. Kleinman, "Nonlinear dielectric polarization in optical media," *Phys. Rev.* **126**(6), 1977–1979 (1926).
26. T. L. Mazely and W. M. Hetherington, "Second-order susceptibility tensors of partially ordered molecules on surfaces," *J. Chem. Phys.* **86**(6), 3640–3647 (1987).
27. C. A. Dailey, B. J. Burke, and G. J. Simpson, "The general failure of Kleinman symmetry in practical nonlinear optical applications," *Chem. Phys. Lett.* **390**, 8–13 (2004).
28. J. F. Ward and P. A. Franken, "Structure of nonlinear optical phenomena in potassium dihydrogen phosphate," *Phys. Rev.* **133**, A183–190 (1964).
29. P. Stoller, P. M. Celliers, K. M. Reiser, and A. M. Rubenchik, "Quantitative second-harmonic generation microscopy in collagen," *Appl. Opt.* **42**(25), 5209–5219 (2003).
30. S. V. Plotnikov, A. C. Millard, P. J. Campagnola, and W. A. Mohler, "Characterization of the Myosin-based source for second-harmonic generation from muscle sarcomeres," *Biophys. J.* **90**, 693–703 (2006).
31. M. Born and E. Wolf, *Principles of Optics*, 6th ed., Oxford, Pergamon Press, London (1993).